

Article

A Geomorphic Approach for Identifying Flash Flood Potential Areas in the East Rapti River Basin of Nepal

Til Prasad Pangali Sharma ^{1,2}, Jiahua Zhang ^{1,2,*}, Narendra Raj Khanal ³, Foyez Ahmed Prodhana ^{1,2,4}, Lkhagvadorj Nanzad ^{1,2,5}, Da Zhang ^{1,2} and Pashupati Nepal ³

¹ Key Laboratory of Digital Earth Sciences, Aerospace Information Research Institute (AIR), Chinese Academy of Sciences (CAS), Beijing 100094, China; tilsharma@radi.ac.cn (T.P.P.S.); foyez@radi.ac.cn (F.A.P.); Lkhagvaa@radi.ac.cn (L.N.); zhangda@radi.ac.cn (D.Z.)

² University of Chinese Academy of Sciences, Beijing 100049, China

³ Central Department of Geography, Tribhuvan University, Kathmandu 66613, Nepal; nrkhanal.geog@gmail.com (N.R.K.); pashupati.nepal@cdg.tu.edu.np (P.N.)

⁴ Department of Agricultural Extension and Rural Development, Bangabandhu Sheikh Mujibur Rahman Agricultural University, Gazipur 1706, Bangladesh

⁵ National Remote Sensing Center, Information and Research Institute of Meteorology, Hydrology, and Environment (IRIMHE), Ulaanbaatar 15160, Mongolia

* Correspondence: zhangjh@radi.ac.cn

Abstract: Basin geomorphology is a complete system of landforms and topographic features that play a crucial role in the basin-scale flood risk evaluation. Nepal is a country characterized by several rivers and under the influence of frequent floods. Therefore, identifying flood risk areas is of paramount importance. The East Rapti River, a tributary of the Ganga River, is one of the flood-affected basins, where two major cities are located, making it crucial to assess and mitigate flood risk in this river basin. A morphometric calculation was made based on the Shuttle Radar Topographic Mission (SRTM) 30-meter Digital Elevation Model (DEM) in the Geographic Information System (GIS) environment. The watershed, covering 3037.29 km² of the area has 14 sub-basins (named as basin A up to N), where twenty morphometric parameters were used to identify flash flood potential sub-basins. The resulting flash flood potential maps were categorized into five classes ranging from very low to very high-risk. The result shows that the drainage density, topographic relief, and rainfall intensity have mainly contributed to flash floods in the study area. Hence, flood risk was analyzed pixel-wise based on slope, drainage density, and precipitation. Existing landcover types extracted from the potential risk area indicated that flash flood is more frequent along the major Tribhuvan Rajpath highway. The landcover data shows that human activities are highly concentrated along the west (Eastern part of Bharatpur) and the east (Hetauda) sections. The study concludes that the high human concentrated sub-basin “B” has been categorized as a high flood risk sub-basin; hence, a flood-resilient city planning should be prioritized in the basin.

Keywords: morphometric analysis; flash flood; Geographic Information System (GIS); remote sensing; SRTM



Citation: Pangali Sharma, T.P.; Zhang, J.; Khanal, N.R.; Prodhana, F.A.; Nanzad, L.; Zhang, D.; Nepal, P. A Geomorphic Approach for Identifying Flash Flood Potential Areas in the East Rapti River Basin of Nepal. *ISPRS Int. J. Geo-Inf.* **2021**, *10*, 247. <https://doi.org/10.3390/ijgi10040247>

Academic Editors: Wolfgang Kainz and Raffaele Albano

Received: 13 February 2021

Accepted: 4 April 2021

Published: 8 April 2021

Publisher's Note: MDPI stays neutral with regard to jurisdictional claims in published maps and institutional affiliations.



Copyright: © 2021 by the authors. Licensee MDPI, Basel, Switzerland. This article is an open access article distributed under the terms and conditions of the Creative Commons Attribution (CC BY) license (<https://creativecommons.org/licenses/by/4.0/>).

1. Introduction

Flood is one of the major disasters that threaten human lives and causes property losses worldwide. Natural disasters have caused severe property damages worth over 1.5 trillion USD in Asia during the last 50 years, where flood shares more than one-third (517 billion USD) of total loss [1]. Several studies have shown that the havoc caused by flood has intensified over the recent past [1–5]. Floods are mainly characterized into two groups namely coastal, and inland flood [6], while inland flood can be further subdivided into various categories, where flash flood is considered as the most complex category [7]. Flash floods are caused by short, sudden intense rainfalls [8], a rapid meltdown of snow,

an outburst of glacial lakes, and lake blockage by a landslide. However, this study focuses on the high-intensity rainfall-induced flash flood that may last for an hour after an intense rainfall posing a dire threat to small-scale catchments [9], being more prominent in magnitude than any other types of events [4,10]. Flash floods have inflicted more than 34 million people in the last 50 years, with a death toll of more than 22,743 people and 34 billion USD worth of damage only in Asia [1]. Hence, identifying flash flood-prone areas has been gaining higher attention than before [3,11,12] which is also the leading step towards flood disaster management. Recently made-available datasets and technologies (satellite data and GIS), including drones [13], provide suitable spatial and temporal accuracy [14] that ultimately lead to a better flood risk reduction.

Flash floods are primarily associated with violent convection storms with a short duration falling over a small area [15]. Heavy rain showers on the area with the steep slopes is one of the most destructive disasters in Nepal that have eradicated many buildings, roads, bridge, and farmland [16]. The existing climate change scenarios suggest that climate extremes (floods) are expected to heighten in the Hindu Kush Himalaya Region [17] mainly due to high-intensity precipitation events [18]. Already inflicted with flood, the area is expected to increase flood frequency and intensity in the future [17]. Therefore basin-scale and cross-boundary watershed management plans are required for flood risk reduction [19].

The onset of a flash flood, its extent and duration, as well as the induced death-toll and property damage, have been analyzed by Terti, et al. [20] in the United States. Saharia, Kirstetter, Vergara, Gourley, Hong, and Giroud [3] have proposed a new model to measure flash flood severity based on geomorphological and climatological variables. Likewise, different aspects of the flash flood hazard have been studied worldwide yet, basin morphology, which is one of the main controlling factors for flood hazard, has not been adequately emphasized [21]. Various watershed conditions, including existing geomorphology, and meteorological conditions, are major determinants of flood re-occurrence [21]. Along with basin geomorphology, anthropogenic activities control the flood impact [22]. Unbridled development of urban space has increased the population exposure to flash floods, making them a serious threat to society at present [23,24]. Monsoon flash floods are mainly attributed to the ground's inability to absorb the excessive water from intense rainfall bursts.

There is a growing body of literature that recognize the importance of flood risk analysis for human societies, where flood risk has been evaluated by utilizing hydrologic and hydraulic modelling [25,26]; where detection of the hazard-prone areas is one of the major steps towards risk reduction. Various methods have been used in flash flood identification and assessment and evaluation [9,27–29]. Hydrological and geomorphic approaches are two mainly used flood risk delineation approaches, while both approaches have certain advantage and drawbacks [27]. Threshold-based flash flood delineation has been used mainly in the ungauged basins with reference to the flash flood guidance [9]. Satellite data along with a multi-criteria decision-making technique, has been used for flood delineation in Romania [12]. Even though an ample number of hydrologic and hydraulic models have also been proposed [29], the traditional methods are usually time-consuming with serious uncertainties [12]. However, the morphometric approach is more useful for preliminary flood delineation, especially in the ungauged basins and in areas where hydrological simulations are not a viable option [28,30]. In addition, the current geomorphic condition of a basin plays an important role in evaluating flash floods and identifying risk-prone areas [12,31,32]. Therefore, the geomorphometric condition of a basin is a widely-used parameter to evaluate the hydrological response of a given watershed [21,33]. Hence, we have utilized geomorphic parameters such as the drainage network, basin geometry, drainage texture, and topographic relief characteristics in this study.

Even though better rainfall-runoff simulations can facilitate flood forecasting accuracy [34], Nepal does not have an ample number of hydrological stations for flood forecasting, which is much fewer than the World Meteorological Organization (WMO) recommends [15]. Moreover, the available meteorological datasets in Nepal are not suf-

ficiently trust-worthy [35]. The inadequate spatial coverage of hydrological databases challenges accurately floods forecasting and flood risk management in Nepal [34]. Hence, accurate flood potential maps are essential to reduce disaster impact, especially for city planners. A study was carried out by Smakhtin and Shilpakar [36] in the East Rapti River Basin with a hydrologic desktop environmental flow assessment method which was not suitable for immediate application. Given that watershed geomorphology is essentially important when the basin undergoes heavy rainfalls, we considered several morphometric parameters in this study to identify flash flood potential areas [21,33,37]. A standard set of morphometric parameters necessary for flash flood susceptibility mapping has not been defined clearly, whereas a combination of various morphometric parameters has been used for flash flood mapping [33,37–39].

During the last few decades, the empirical studies on flash flood forecasting [40,41], and flood risk management [34,42] in Nepal have been accumulated, but surprisingly, there is limited attention to morphometric analysis identify flood potential at the basin level. Against this backdrop, this paper highlights geomorphological approaches based on the satellite remote sensing data to identify flash flood potential areas in the East Rapti River basin. In particular, this study aims to (1) examine the relationship between morphometric parameters with a flash flood in East Rapti River basin; and (2) develop a complete flood susceptibility map for the study area.

2. Study Area

Nepal is located in the central Himalaya region and shares border with India from three sides and China to the north (Figure 1). A steep topographic gradient with intense rainfalls causes flash floods in Nepal [43]. The country has three major river basins namely: Koshi, Gandaki, and Karnali. There are still myriad small watersheds in Nepal's southern plain (Figure 1). The East Rapti River, a tributary of the Gandaki river basin, originates in the Mahabharat mountain range and joins the Narayani River (Figure 1). Based on the 30-m Shuttle Radar Topographic Mission (SRTM) Digital Elevation Model (DEM) data, the basin elevation extends from 140 m at its conjunction to 2586 in the north, with a total area of 3037.29 square kilometers. Based on International Centre for Integrated Mountain Development (ICIMOD) landcover data [44], the forest covers more than 65.91 percent of the total basin, followed by croplands (28.53 percent). The basin is one of the highly populated basins in Nepal with a growing population and urbanization in its two major growing cities of east Bharatpur and Hetauda. The basin includes thirty-two Village Development Committees (VDCs) from Chitwan district and twenty-three out of 43 VDCs from Makwanpur districts. Agriculture is the dominant occupation in the local population, followed by technical services [45]. The basin also has scattered settlements both in Makwanpur and Chitwan districts [46].

Being one of the flood-affected countries, Nepal is prone to massive casualties and property damages of floods. To map the flood disaster, we used Disability Adjusted Life Years (DALYs) developed by World Health Organization (WHO) [47], which was later used in disaster loss measurement [48]. The DALY converts all types of damages into human life years, which makes it easy to compare disaster damage over space (Figure 1). Floods initiate in the basin almost every year during the monsoon season [19]. In retrospect, the year 2017 was marked with severe floods. Approximately 12 flood events were recorded in the study area, where 563 families were affected, and six people were lost. A severe flood occurred from 12 to 14 August 2017. Six flood events were recorded in the basin from 10 to 12 July 2019 alone, where two people were lost, and ten households were affected by the event [49]. Recent studies suggest a rise in urban flooding events [6,50]. Therefore, flood potential area identification is essential for flood risk reduction and flood resilient city development [51].

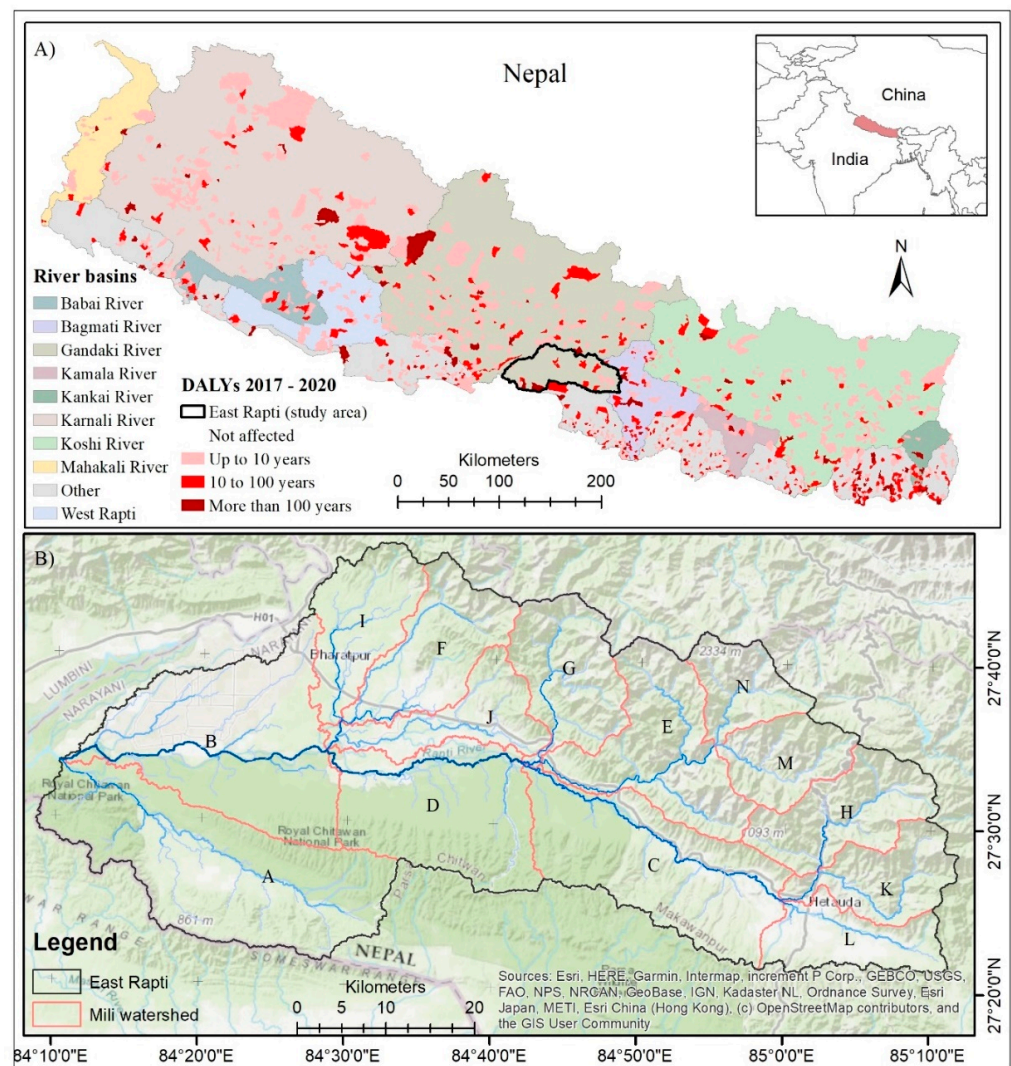


Figure 1. (A) Map of showing major river basins and Disability-Adjusted Life Years due to flood loss (2017 to 2020) in Nepal, and (B) The study area: East Rapti River Basin.

Monsoon is responsible for 88 percent of total annual precipitation concentrated from June to September [16]. The East Rapti River basin receives about 150 mm in pre-monsoon, 2000 mm in monsoon, 80 mm in post-monsoon, and 20 mm during the winter season [16]. High precipitation and steep topographic gradient (especially steep, narrow river beds) are two main characteristics of the basin (Figure 1).

3. Materials and Methods

3.1. Morphometric Parameters

This study has used 20 morphometric parameters, categorized into four classes: Drainage Network, Basin Geometry, Drainage Texture Analysis, and Relief Characteristics (Figure 2). Each parameter was calculated using the corresponding equations presented in Table 1. All the calculations related to morphometric parameters were done in the GIS environment. Among these parameters, the basin area is directly related to discharge as the bigger the drainage basin, the higher the amount of precipitation it receives, hence generates higher runoff [37]. Various topographic parameters, including elevation, basin slope, and roughness number, directly affect the flash floods [11]. A basin with a steep slope has a relatively higher number of flash floods than a basin with a gentle slope [52]. The roughness number is the product of drainage density and relief, where values <1 indicate a smooth topography, a value ranging between 1 and 2 represents sharp topography, while

a value above 2 indicates that the area is poorly cemented [53]. Therefore, high surface roughness reduces runoff velocity by providing a greater time for surface infiltration and water recharge [33].

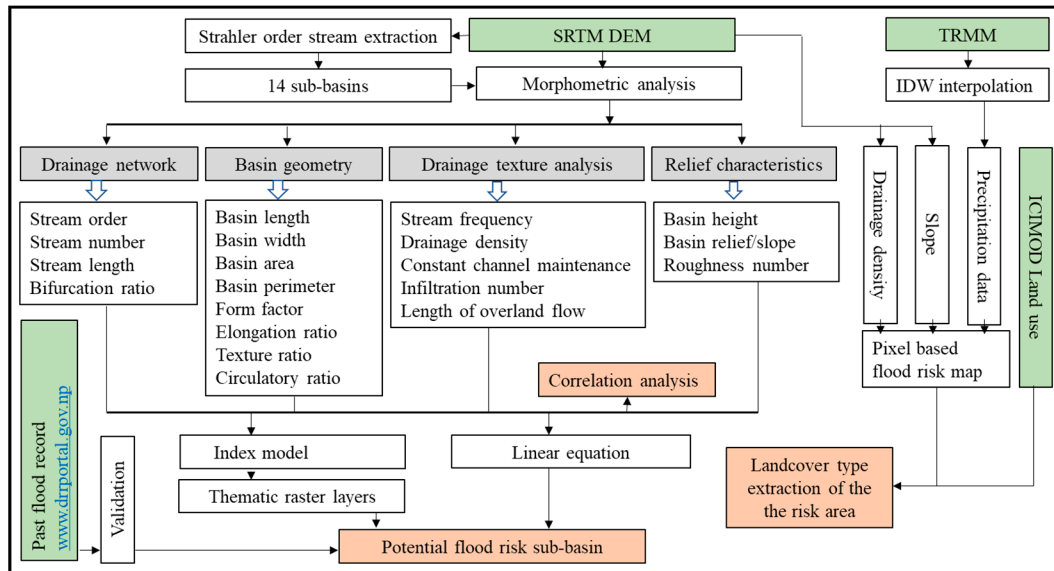


Figure 2. Flowchart of the applied methodology.

The elongation ratio is the proportion between the basin's diameter and maximum length with an inverse relationship with flash floods [54]. In other words, basins with a smaller elongation ratio discharge more runoff and vice versa. The elongation ratio varies between 0 and 1, where the maximum value (close to 1) indicates low basin relief [54]. The circulatory ratio is the ratio between circumference and perimeters of a basin, with a positive correlation with runoff [55]. The ratio between watershed diameter and length was calculated as the elongation ratio (L_e) [54]. The form factor indicates the drainage basin's shape with lower values indicating an elongated basin shape [33]. The circulatory ratio is the ratio between basin's area to its perimeter [55]. The drainage texture is derived from the number of streams divided by its perimeter [54]. Likewise, the stream frequency is calculated as the total stream segments from all orders per unit area [56] (Table 1).

Additionally, river system properties also affect runoff generation, which is positively correlated with stream numbers [11,57] and total stream length [57]. The stream frequency is the number of streams per unit area, while drainage density is the ratio of total stream length to basin's area [56]. The stream frequency and drainage density both positively correlated with total runoff [37]. A watershed with a lower drainage density has a better infiltration, while high stream frequency implies lower infiltration capacity [11]. The contribution of drainage density and stream frequency to the overall flow is lower compared with morphometric characteristics between small and large basin [56]. The bifurcation ratio is defined as the average number of branching of streams of a given order to that of streams of the next order [56]. The mean bifurcation ratio is important to characterize the overall stream system over various basins [57]. This parameter has an inverse relationship with runoff generation [11].

Mapping Flash Flood Risk Areas

The East Rapti River basin has 14 sub-basins (Figure 1B). Flood risk in the basin was analyzed at two different spatial scales: sub-basins, and sub-watershed. For sub watershed risk evaluation, 20 morphometric parameters were calculated in the GIS environment. Two different methods (index model, and hazard degree calculation) were applied to derive potential flood risk areas (Figure 2). Under the index model, we assigned values (1 to 5) for

each morphometric parameter based on their relation to flash floods. The Jenks Natural Breaks Classification (JNBC) method [58] was used where value 1 was assigned to the low-risk and 5 to the high-risk areas. The JNBC method seeks to minimize an average deviation from the mean class while maximizing the deviation from other group's mean. After assigning the values, we rasterised the corresponding thematic layers, and finally used the overlay function in the GIS environment to get the final potential flood risk sub-basins of the East Rapti River. In addition to index modelling, flash flood risk was estimated by hazard degree calculation linear interpolation techniques [59], where if the value of the morphometric parameter is positively correlated with flash flood occurrence, we used Equation (1); otherwise, we used Equation (2). Finally, we compared derived flood risk sub-basin with past flood records of the basin to validate the result.

Twelve thematic flood risk maps were prepared based on the ranks obtained from the morphometric analysis, which were later used to derive the flash flood risk area over 14 watersheds. The final map was categorized into five risk classes: very low, low, intermediate, high, and very high. In addition to basin-wide risk analysis, we have used slopes, drainage density, and rainfall to analyze flood risk per square kilometer area. In this way, we identified flood risk in two spatial scales, which will be discussed in the result and discussion section.

$$\text{Hazard degree} = \frac{4(X - X_{min})}{X_{max} - X_{min}} + 1 \quad (1)$$

$$\text{Hazard degree} = \frac{4(X - X_{max})}{X_{min} - X_{max}} + 1 \quad (2)$$

where X represents the value of morphometric parameters to estimate for flood risk for each basin.

Table 1. Morphometric parameters used in the study.

No	Parameters	Equations	Reference
A. Drainage Network			
1	Stream Order (u)	Strahler stream order	[53]
2	Stream number (N_u)	$N_u = N_1 + N_2 + \dots + N_n$	[56]
3	Stream length (L_u)	$L_u = L_1 + L_2 + \dots + L_n$	[57]
4	Bifurcation ratio (R_b)	$R_b = \frac{N_u}{N_{u+1}}$	[57]
B. Basin geometry			
5	Basin length in km (L_b)	$L_b =$ <i>highest length of the basin</i>	[60]
6	Basin width in km (W_b)	$W_b =$ <i>highest width of the basin</i>	[60]
7	Area in km (A)	A	[54]
8	Perimeter in km (P)	P	[54]
9	Form factor (R_f)	$R_f = \frac{A}{(L_b)^2}$	[56]
10	Elongation ratio (L_e)	$L_e = 2\sqrt{\left(\frac{A}{\pi}\right)}/L_b$	[54]
11	Texture ratio (T)	$T = N_1/P$	[54]
12	Circulatory ratio (R_c)	$T = 4\pi A/P^2$	[55]
C. Drainage texture analysis			
13	Stream frequency (F_s)	$F_s = \sum N_u/A$	[56]

Table 1. Cont.

No	Parameters	Equations	Reference
14	Drainage density in km/km ² (D_d)	$D_d = \sum L_u / A$	[56]
15	Constant channel maintenance (C)	$C = 1/D_d$	[54]
16	Infiltration number (I_f)	$I_f = D_d \times F_s$	[61]
17	Length of overland flow in km (L_g)	$L_g = 1/(2D_d)$	[56]
D. Relief characteristics			
18	Basin height in km (B_h)	$B_h = Z_x - Z_m$	[53]
19	Basin relief/slope in km (R_h)	$R_h = B_h/L_b$	[54]
20	Ruggedness number (R_n)	$R_n = B_h \times D_d$	[53]

3.2. Data Used

This study was mainly based on satellite remote sensing data. Since the study focused on geomorphological parameters to identify flood potential areas, the Shuttle Radar Topographic Mission (SRTM) Digital Elevation Model (DEM) data with a spatial resolution of 30 meters was used in this study. The SRTM DEM data has been widely used in various research fields, including geology, geomorphology, hydrology, glaciology, the study of various natural hazards, and vegetation surveys [62]. The SRTM DEM has a high spatial resolution which is crucial for flood disaster studies and various hydrologic modelling [63]. Two tiles of the SRTM DEM (n27e84, and n27e85) were downloaded from the Earth Explorer (<https://earthexplorer.usgs.gov>, accessed on 29 November 2019). To delineate watersheds, DEM sinks were removed as the preprocessing steps. Considering the East Rapti River conjunction with the Narayeni River, the river basin and stream networks were delineated using surface flow direction (the D8 flow direction algorithm) [64] in the QGIS environment. Next, streams' Strahler orders were extracted, and only those with orders of greater than 7 were kept. The East Rapti River Basin was further subdivided into 14 watersheds by assigning 90 square kilometers as the minimum area.

Existing land uses and landcovers are very important while undertaking flood risk reduction. The ICIMOD land cover data was used to extract landcover types of the basin with particular attention to the flash flood potential areas. The ICIMOD land cover data (2010) provides consistent and harmonized national land cover maps for Nepal. The ICIMOD landcover data included 30-meter Landsat TM satellite images of 2009, 2010, and 2011 that were used to classify the land cover [44].

TRMM precipitation data: Tropical Rainfall Measuring Mission (TRMM) precipitation data version 7 (3B42 daily) (DOI:10.5067/TRMM/TMPA/DAY/7) has been used in this study. The data provides information on the spatiotemporal variation in rainfall over the basin. The daily accumulated precipitation product is generated from 3-hourly TRMM Multi-Satellite Precipitation analysis TMPA (3B42). The simple summation of valid 3-hourly TRMM precipitation data was used to retrieve daily precipitation, and the result is presented in mm per day. The TRMM daily precipitation (3B42) product is frequently used in many climates and environmental studies [65,66]. However, the coarse spatial resolution of the precipitation data hinders its application for small river basins [66]. Considering the data limitations (coarse spatial resolution), we took the pixel midpoint value as one station data and interpolated them over the basin. In this process, we extracted data for 15 points covering the basin and applied the Inverse Distance Weighting (IDW) interpolation technique. The IDW interpolation technique is an appropriate method to interpolate precipitation data [67]. The precipitation data were used to visualize flood risk areas in the study basin. For disaster damage data, Nepal disaster reduction risk (DRR) portal is a reliable government source for disaster-related damage in Nepal. Data on a large variety of disasters is available on this portal (<http://drrportal.gov.np>, accessed on 15 December

2020) which can be download in excel file format. Downloaded flood damage data were spatially presented in the map to see its spatial variations (Figure 1A).

The morphometric analysis has widely and successfully been used to identify potential flash floods over various river basins [11,37,68]. Basin geomorphology is a complete system where the hydrologic and morphometric factors are interrelated [21]. Hence, the correlation coefficients among calculated morphometric parameters were calculated and presented as a correlation matrix, discussed in the result section. Moreover, two different methods (index model and linear hazard degree equation) were used to detect flash flood prone areas, so we can compare their results. Finally, the derived potential flood risk areas were compared with the previous flood disaster loss record of DRR portal of Nepal.

4. Results and Discussions

4.1. Morphometric Analysis

Digital elevation model (DEM) shows the elevation varies from 140 meters at the river confluence (Narayani River) to 2586 meters at its north. The extracted streams mostly show a semi-dendritic drainage pattern, where streams resemble tree branches, are the most common drainage network type that develops where the river channel follows the slope of the terrain [69]. Though the overall stream shows a semi-dendritic drainage pattern, the southern part of the basin shows an irregular drainage pattern (Figure 3b) due to the presence of Siwalik hills composed of unconsolidated materials. The four major branches of the East Rapti show a parallel pattern, and the small branches link the mainstream as the trellis. As the elevation reaches its maximum at its north-eastern section, most streams follow a southerly direction toward the Narayani River. North-east highlands are the upstream of the basin, collecting runoff and posing a threat for downstream areas (Figure 3a).

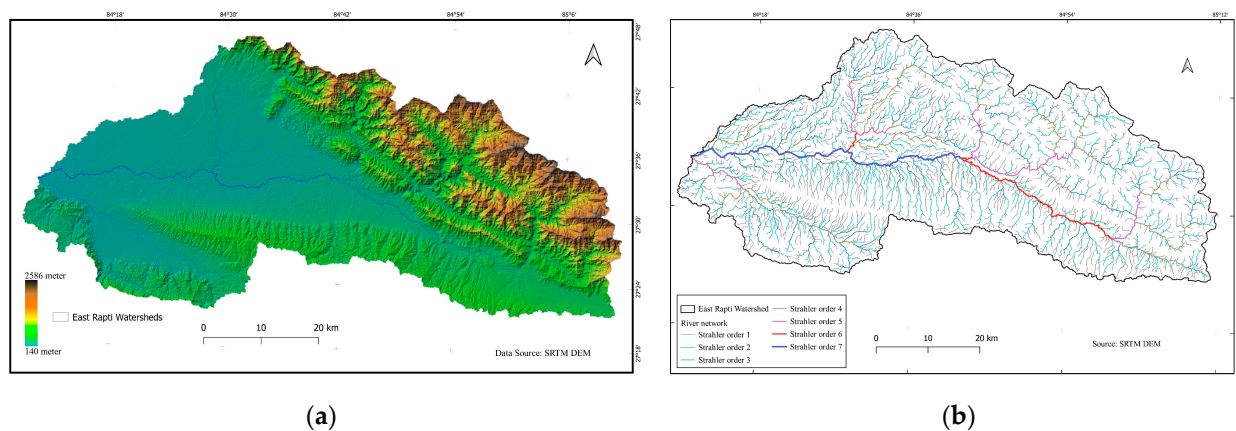


Figure 3. East Rapti basin (a) 30-meter Digital Elevation Model (DEM), and (b) Strahler stream order segments.

The bifurcation ratio (R_b) value of the 14 sub-basins ranged from 4.020 to 5.460 with an average value of 4.717 (Figure 4D). This means that the basin drainage system is less structurally controlled with less geologic distortion [57]. The high bifurcation ratio (for example sub-basin N) shows less surface flow which results in high infiltration and lower flood risk [70]. On the other hand, a high bifurcation ratio is directly associated with the elongation ratio that also tends to reduce flood risk [21]. On the contrary, a low bifurcation ratio with high relief increases the flood risk [33] (for example, sub-basin N).

Schumm [54] has classified elongation value into circular (0.9–1.0), oval (0.8–0.9), less elongated (0.7 to 0.8), elongated (0.5–0.7), and more elongated (less than 0.5) classes. The calculated L_e value shows the study basin constitutes an elongated to oval shape sub-basins: where the sub-basin “J” (0.55) is an elongated basin, while basin “N” (0.90) is categorized as an oval shape. The form factor (R_f) is the ratio of basin area over squared basin length [56]. The calculated form factor for the study basin ranges from 0.24 to 0.64, shows the oval to elongated basin shape (Figure 4G) with an average sub-basin value of

0.386. The circulatory ratio in the studied sub-basin ranges from 0.16 to 0.53 (Figure 4J) with an average of 0.32, showing an elongated watershed shape. The calculated drainage texture (T) of the studied sub-basins basin ranges from 1.13 to 2.64 with an average value of 1.69, referring to a moderate drainage texture. Stream frequency is mainly under the influence of lithology, structures, infiltration, vegetation cover, and relief. Calculated stream frequency ranges from 0.83 in sub-basin H to 1.15 in sub-basin B. Less drainage density value shows high relief [56].

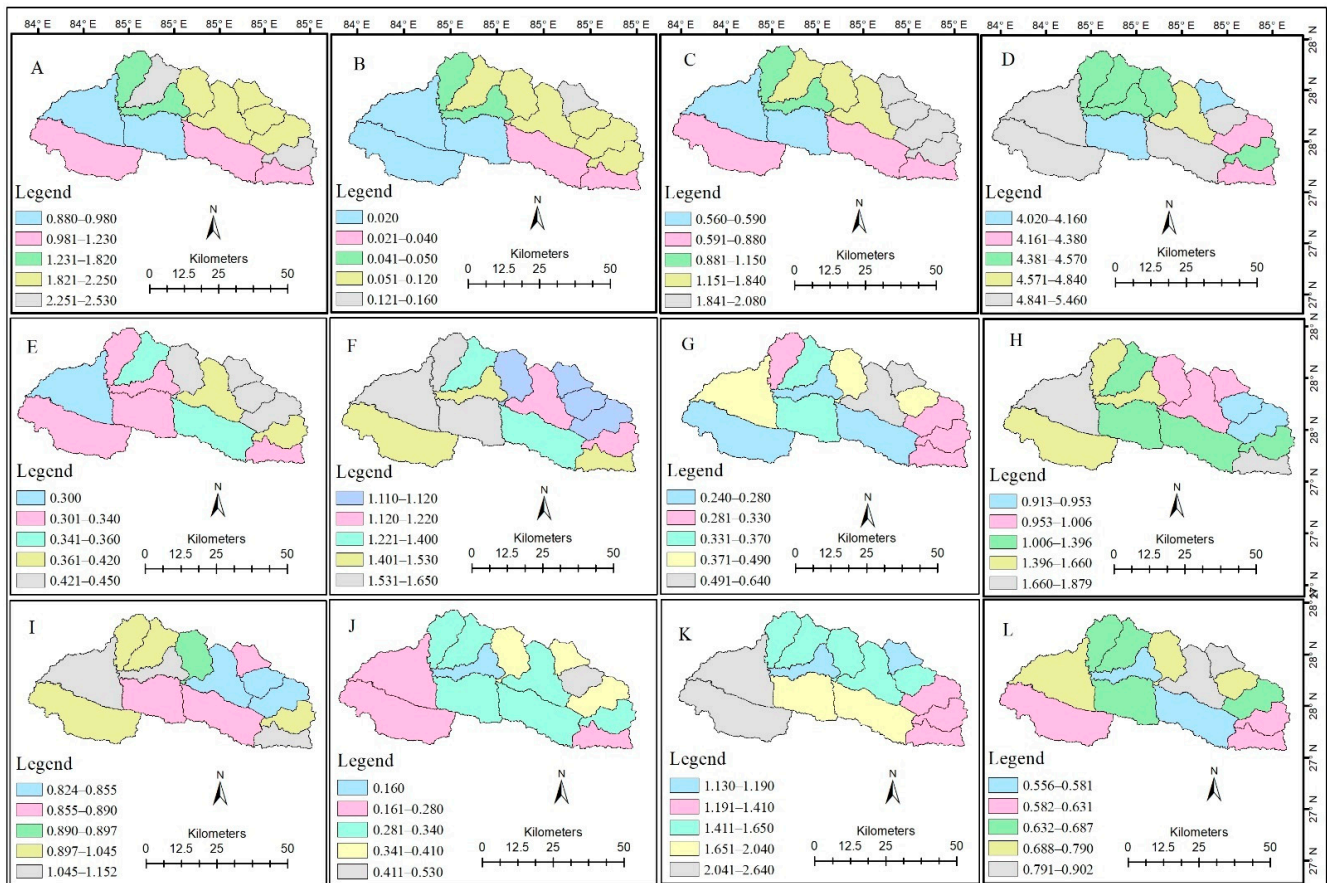


Figure 4. The thematic raster layers (Roughness number (A), Relief ratio (B), Basin Height (C), Bifurcation Ratio (D), Length of overland flow (E), Drainage density (F), Form Factor (G), Infiltration number (H), Stream frequency (I), Circulatory ratio (J), Texture ratio (K), Elongation ratio (L)).

Drainage density (D_d) is an indicator for stream eroded topography [56], which is a very important runoff controlling factor where high value accelerates runoff [33]. The drainage density in the studied sub-watersheds ranges from 1.11 in sub-basin “H” to 1.65 in sub-basin “B” (Table 2). The infiltration number (I_f) was calculated by multiplying drainage density and stream frequency, where higher the infiltration number shows higher runoff and vice versa [61]. The calculated infiltration numbers in the study sub-basin range from 0.913 in sub-basin “H” to 1.88 in the sub-basin “B” (Figure 4F).

The maximum and minimum height of a sub-basin was used to calculate basin height (B_h). Basin height in the studied sub-basin ranges from 0.56 in the sub-basin “D” to 2.08 in the sub-basin “K” (Figure 4C). Likewise, the relief ratio (R_h) was derived by dividing basin relief by the total length of the basin (Table 1). The relief ratio represents the degree of general steepness, which also indicates the rate of soil erosion in the basin [54]. The calculated R_h value ranges from 0.02 in the sub-basin “C” to 0.16 in the sub-basin “N”, with an average value of 0.068. In addition to that, Ruggedness number (R_n) is an indicator of slope roughness of the basin [53], where the value ranges from 0.88 in the sub-basin “D”

to 2.53 in the sub-basin “K” with the mean value of 1.76 in the overall study area (Table 2). The length of overland flow in the study basin ranges from 0.30 in the sub-basin “B” to 0.45 in the sub-basin “N”. Less value for overland flow length (L_g) indicates fast runoff and high-water accumulation [33,56].

Table 2. Tabulated parameters value of the study area.

	N	M	L	K	J	I	H	G	F	E	D	C	B	A
U	5	5	5	5	5	5	5	6	6	5	7	6	7	5
N_u	130	157	220	203	228	250	215	250	269	338	427	490	768	745
L_u	108.33	129.06	191.34	160.74	201.19	252.71	190.88	194.8	255.04	291.8	478.9	478.31	689.42	687.68
L_b	12.38	16.18	20.41	20.54	23.48	21.95	22.88	20.09	22.18	20.18	28.62	35.89	29.17	40.36
W_b	13.51	11.49	8.99	8.47	10.61	11.33	10.27	14.2	10.34	22.58	18.41	12.28	19.64	14.74
A	97.86	115.74	124.96	131.97	133.92	159.58	172.27	173.76	181.73	247.58	303.74	341.51	416.94	462.95
C	0.903	0.897	0.653	0.821	0.666	0.631	0.903	0.892	0.713	0.848	0.634	0.714	0.605	0.673
P	54.65	52.39	78.61	72.32	101.84	80.02	76.03	78.26	86.54	103	105.27	120.36	144.9	144.72
R_b	4.02	5.42	4.38	4.52	4.52	4.54	4.34	4.57	4.48	4.84	4.16	5.35	5.46	5.44
R_f	0.639	0.442	0.3	0.313	0.243	0.331	0.329	0.431	0.369	0.608	0.371	0.265	0.49	0.284
L_e	0.902	0.75	0.618	0.631	0.556	0.649	0.647	0.74	0.686	0.88	0.687	0.581	0.79	0.602
T	1.189	1.508	1.399	1.41	1.129	1.562	1.407	1.597	1.56	1.65	2.014	2.036	2.643	2.577
R_c	0.412	0.53	0.254	0.317	0.162	0.313	0.374	0.357	0.305	0.293	0.344	0.296	0.25	0.278
F_s	0.889	0.855	1.152	0.977	1.105	0.99	0.824	0.898	0.968	0.852	0.886	0.89	1.137	1.045
D_d	1.107	1.115	1.531	1.218	1.502	1.584	1.108	1.121	1.403	1.179	1.577	1.401	1.654	1.485
I_f	0.984	0.954	1.765	1.191	1.66	1.568	0.913	1.007	1.359	1.004	1.396	1.247	1.88	1.553
L_g	0.452	0.448	0.327	0.411	0.333	0.316	0.451	0.446	0.356	0.424	0.317	0.357	0.302	0.337
B_h	1.96	2	0.75	2.08	1.1	1.15	2.03	1.84	1.75	1.81	0.56	0.88	0.59	0.74
R_h	0.158	0.124	0.037	0.101	0.047	0.052	0.089	0.092	0.079	0.09	0.02	0.025	0.02	0.018
R_n	2.17	2.23	1.148	2.533	1.653	1.821	2.249	2.063	2.456	2.133	0.883	1.233	0.976	1.099

Parameters are abbreviated as follows: (R_b) mean bifurcation ratio, (L_e) Elongation ratio, (R_f) form factor, (R_c) circularity ratio, (T) texture ratio, (F_s) stream frequency, (D_d) drainage density, (L_g) length of overland flow, (I_f) infiltration number, (B_h) basin relief, (R_h) relief ratio, (R_n) ruggedness number are used.

The correlation matrix (Figure 5) shows the relationship between the morphometric variables. Blue cells in the matrix show a positive correlation, while the grey cells show a negative correlation. The I_f , D_d , F_s , T, R_b , and C, have a positive relationship with all other variables except P, R_f , L_e , and R_c . On the other hand, L_g , B_h , R_h , and R_n have an inverse relationship with all morphometric parameters except P, R_f , L_e , R_c , L_g , B_h , R_h , and R_n (Figure 5).

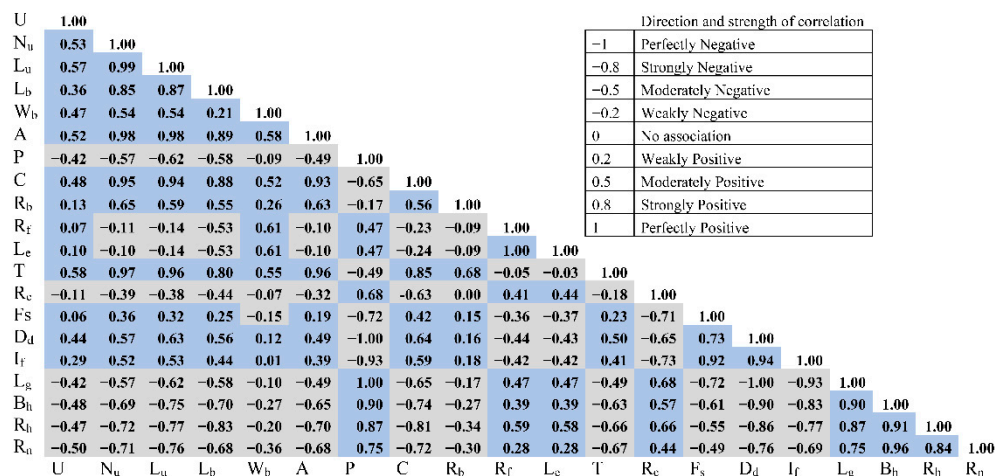


Figure 5. Correlation matrix of calculated morphometric parameters in the study area.

4.2. Mapping Flash Flood Potential Areas

Based on the calculated geomorphic parameters, two different methods: raster overlay through the index model and linear equation [56], have been used to identify areas at risk of flood. All morphometric parameters that have been used in this study (Table 1) have a positive relationship with flood hazard, except bifurcation ratio (R_b) and the length of overland flow (L_g), as they have an inverse relationship with runoff (Table 3). Based on morphometric parameters relationship with runoff, two linear equations have been used: Equations (1) and (2) were used for those parameters with a positive and negative relationship with runoff, respectively. The obtained flood risk index is categorized into five groups from very low to very high (Figure 6; Table 3).

Calculated morphometric values were grouped into five different weights (1 to 5) [33] in terms of flood risk. The flood risk in the sub-basins is categorized as very low (c), low (H), intermediate (A, D, J, and M), high (D, E, K, and L), very high (B, I, F, and N). However, linear equation-based flood risk analysis categorized the basin risk differently: very low (C), low (A and H), intermediate (D, I, G, and M), high (I, E, L, and K), and very high (B, F, and N) (Figure 6). The raster overlay function was applied after assigning risk values to the particular sub-basins (Figure 4), and the overall flood potential risk map was generated (Figure 6).

Table 3. Assigned weights (index) to morphometric parameters in terms of flash flood potential.

Factor	Class	Weight	Factor	Class	Weight
(A) Roughness number (R_n)	0.880–0.980	1	(G) Form factor (R_f)	0.240–0.280	1
	0.981–1.230	2		0.281–0.330	2
	1.231–1.820	3		0.331–0.370	3
	1.821–2.250	4		0.371–0.490	4
	2.250–2.530	5		0.491–0.640	5
(B) Relief ratio (R_n)	0.020	1	(H) Infiltration number (I_f)	0.913–0.953	1
	0.021–0.040	2		0.954–1.006	2
	0.041–0.050	3		1.007–1.396	3
	0.051–0.120	4		1.397–1.660	4
	0.121–0.160	5		1.661–1.879	5
(C) Basin height (B_n)	0.560–0.590	1	(I) Stream frequency (F_s)	0.824–0.855	1
	0.591–0.880	2		0.856–0.890	2
	0.881–1.150	3		0.891–0.897	3
	1.151–1.840	4		0.898–1.045	4
	1.841–2.080	5		1.046–1.152	5
(D) Bifurcation ratio (R_b)	4.020–4.160	5	(J) Circulatory ratio (R_c)	0.160	1
	4.161–4.380	4		0.161–0.280	2
	4.381–4.570	3		0.281–0.340	3
	4.571–4.840	2		0.341–0.410	4
	4.841–5.460	1		0.411–0.530	5
(E) Length of overland flow (L_g)	0.300	5	(K) Texture ratio (T)	1.130–1.190	1
	0.301–0.340	4		1.191–1.410	2
	0.341–0.360	3		1.411–1.650	3
	0.361–0.420	2		1.651–2.040	4
	0.421–0.450	1		2.041–2.640	5
(F) Drainage Density (D_d)	1.110–1.120	1	(L) Elongation ratio (L_e)	0.556–0.581	1
	1.121–1.220	2		0.582–0.631	2
	1.221–1.400	3		0.632–0.687	3
	1.401–1.530	4		0.688–0.790	4
	1.531–1.650	5		0.791–0.902	5

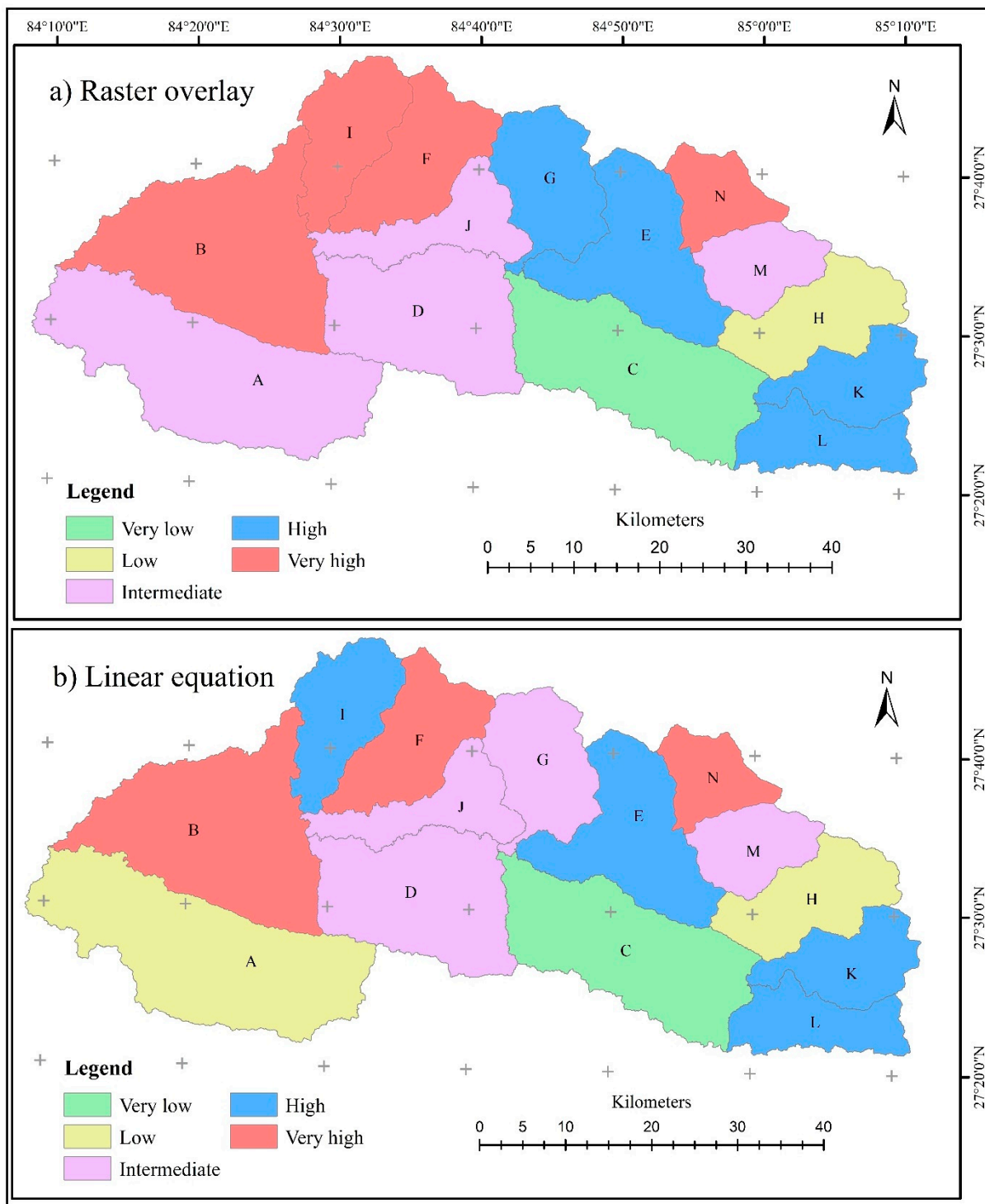


Figure 6. Flash flood potential areas (a) raster overlay (b) linear equation.

4.3. Linear Equation-Based Risk Mapping

In addition to the index model, flood risk potential was estimated by applying a linear interpolation technique, which was first proposed by [59]. Equations (1) and (2) were used to calculate flood risk from the extracted geomorphic parameters, and the obtained values are presented in Table 4.

Table 4. Result derived from linear equation-based risk mapping.

	R_b	R_f	L_e	T	R_c	F_s	D_d	I_f	L_g	B_h	R_h	R_n	Sum	Degree
N	5.000	4.995	5.000	1.159	3.714	1.789	1.000	1.293	1.000	4.684	5.009	4.119	38.763	5
M	1.111	3.011	3.248	2.001	5.000	1.379	1.059	1.168	1.088	4.789	4.017	4.266	32.137	3
L	4.000	1.576	1.716	1.714	1.999	5.000	4.105	4.523	4.353	1.500	1.536	1.643	33.664	4
K	3.611	1.705	1.868	1.743	2.684	2.868	1.812	2.147	2.103	5.000	3.379	5.001	33.922	4
J	3.611	0.999	1.000	1.000	1.000	4.424	3.893	4.091	4.185	2.421	1.824	2.866	31.314	3
I	3.556	1.891	2.080	2.144	2.642	3.022	4.488	3.709	4.642	2.553	1.983	3.274	35.983	5
H	4.111	1.869	2.055	1.735	3.309	1.000	1.008	1.000	1.011	4.868	3.021	4.312	29.300	2
G	3.472	2.894	3.133	2.237	3.114	1.896	1.103	1.386	1.152	4.368	3.103	3.860	31.717	4
F	3.722	2.277	2.501	2.138	2.552	2.758	3.169	2.845	3.556	4.132	2.740	4.813	37.204	5
E	2.722	4.686	4.747	2.377	2.425	1.341	1.524	1.377	1.735	4.289	3.048	4.031	34.305	4
D	4.611	2.291	2.516	3.337	2.982	1.748	4.438	2.999	4.605	1.000	1.045	1.000	32.572	3
C	1.306	1.224	1.288	3.395	2.458	1.803	3.149	2.380	3.537	1.842	1.186	1.847	25.414	1
B	1.000	3.495	5.000	1.159	3.714	4.811	5.000	5.000	5.000	1.079	1.064	1.224	38.328	5
A	1.056	1.416	3.248	2.001	5.000	3.697	3.770	3.647	4.083	1.474	1.010	1.524	30.285	3

The result shows that the sub-basins B, F, and N fall into the very high loss class while sub-basins I, F, L, and K fall into the high flood risk (Figure 6) basins that correspond with the past flood record (Figure 7). On the other hand, the sub-basin C was categorized as a very low flood risk zone in both types of risk calculation, where no flood recorded since 2018 (Figure 7). As for the sub-basins I and A, they were categorized differently with the two methods. Basin “I” was categorized as a very high-risk sub-basin by index modeling but as a high-risk sub-basin by linear equation-based risk mapping. Likewise, the sub-basin A was categorized as an intermediate risk area by the linear equation while as a low flood risk area by the linear interpolation (Figure 6). The different risk categories for sub-basin “I” and “A” can be attributed to different model structures [33]. Overall, the flash flood potential map (Figure 6) corresponds to the past flood record map (Figure 7).

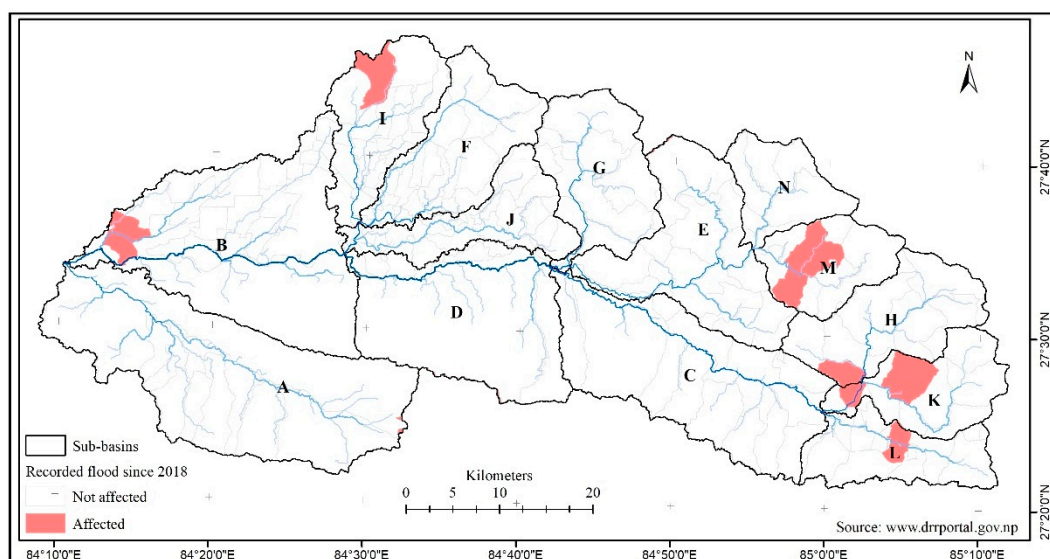


Figure 7. Recorded recent flood event in the study area (flood event source: www.drrportal.gov.np accessed on 25 November 2020).

4.4. Pixel Wise Flash Flood Risk Identification

Although the previous findings (Figure 6) shed light on flood risk in the sub-basin, they did not provide any spatial details for planners. A very high-risk sub-basin “N” might not be entirely exposed to floods. Therefore, detailed risk identification was necessary to examine flash flood potential risk per square kilometer pixel using drainage density, slope, and rainfall data.

TRMM precipitation data was used to see the relationship between three parameters: slope, DD, and precipitation. Southern sub-basins with gentle slopes received underwent heavy rainfall on 17 July 2019 (Figure 8a). On the contrary, the northern sub-basins with a rugged topography received comparatively less precipitation. This is just an example, while many parts of the country receive intense precipitation during the monsoon season. The calculated drainage density and slope values are illustrated in Figure 8b,c. Compiling precipitation, drainage density, and the slope map, we derived the flash flood risk pocket area (Figure 8d).

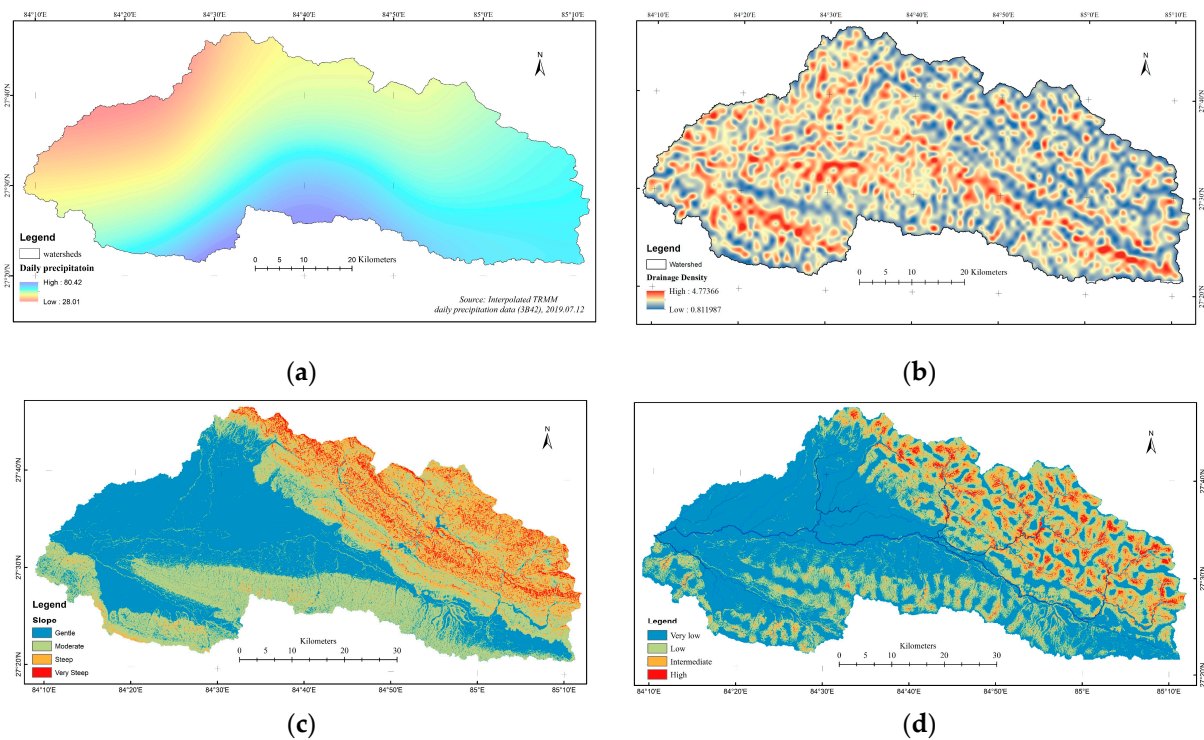


Figure 8. Consists of (a) Tropical Rainfall Measuring Mission (TRMM) precipitation distribution, (b) drainage density (Km/km²), (c) Slope, and (d) Overall flash flood potential area.

Rainfall, drainage density, and slope are mainly related to flood risk. On the other hand, high rainfall in the area of high drainage density and the steep slope has less chance of infiltration, which leads to larger amounts of runoff and hence flood risk. Unlike inundation and riverbank flooding, flash flood potential is higher upstream along with the Tribhuvan Rajpath, with steep topography and excessive rainfall. Receiving heavy precipitation in the southern part with a gentle slope, however, does not lead to serious flash flood incidents.

Land Cover Type under Flood Risk Areas

Proper land-use planning is essential for flood risk reduction [50]. The ICIMOD land use data has been used to extract land cover classes of the flood risk area. Forest, cropland, barren land, grassland, built-up area, waterbody, and shrubland classes are present in the East Rapti River basin. Having Chitwan National park in the basin, the majority of the basin is then covered by forest (65%), followed by cropland (28%). Having

scattered settlements, particularly in the form of separate rural houses, make the landcover of negligible importance (Figure 9). However, approximately 26 square kilometers area in the basin is grouped as buildup areas. The built-up areas located in the flood-prone sub-basins are categorized as very high (sub-basin B) and high (sub-basin K, and L) classes. Croplands are the second-highest land cover type in the study basin, which are mostly concentrated in high-risk areas. Considering the present landcovers in the flood prone areas as well as, the fragile location of the major cities, the government needs to give more attention to city planning in the East Rapti River basin. Because the main cause that triggers urban flood (besides rainfall intensity) are the unplanned urban sprawl along the stream banks, the human interference in the main streams altering the hydraulic stream characteristics and the failures of technical works (bridge, or culverts), in combination with the possible deforestation [24,71,72].

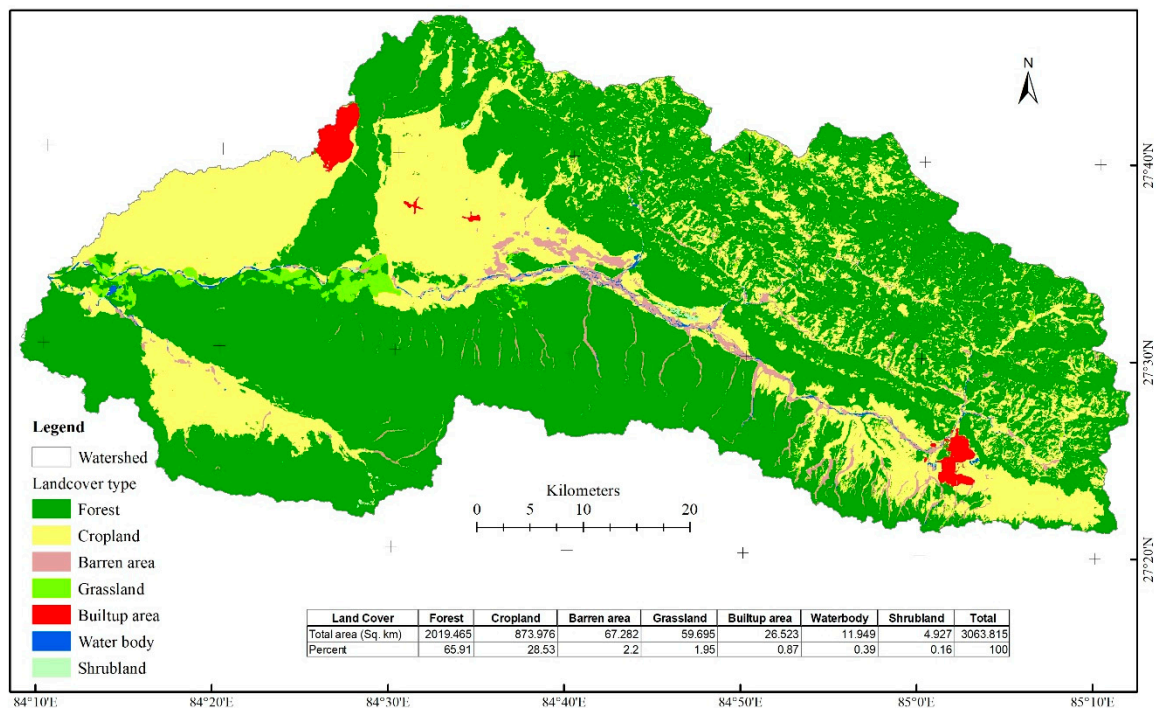
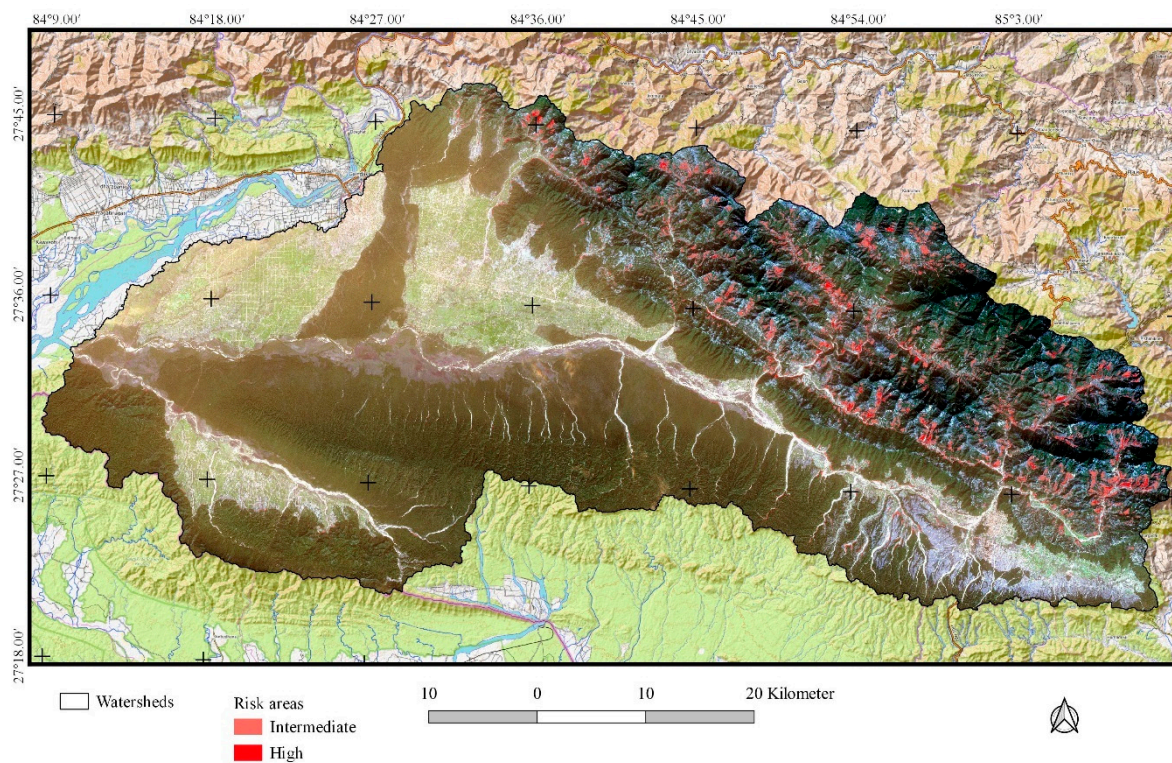


Figure 9. Existing land cover types in the study area. Adapted with permission from Kabir Uddin [44] Copyright 2014 Elsevier Ltd.

We overlaid the flash flood potential compact area and the ICIMOD landcover map to identify various landcover types exposed to flood risk (see Table 5). Among all land cover types, Built-up areas, croplands, and grasslands are the major sources of concern for local livelihood. Hence, we have displayed these landcover types in the following Figure 10. Sum 2.53 percent out of the total area is at high flood risk where croplands is at high risk of flood. Given that the isolated residential areas were not captured in the LULC map, we assumed that there are buildings inside the cropland areas [19]. Ten percent of the total land is at moderate flood risk, with 5 percent of which as croplands. Likewise, thirty percent of the total area, where the 5 percent buildup area exists, is seldom affected by flood (Table 5). Based on this calculation, about 57 percent of the study area is not at risk of flash floods (Table 5).

Table 5. Flash flood potential and existing land cover area.

Land Use Type	High	%	Medium	%	Less	%	Not Affected	%	Grand Total	%
Built up area	0.000	0.00	0.023	0.09	1.453	5.48	25.047	94.43	26.523	0.87
Agriculture land	11.298	1.29	51.400	5.88	147.066	16.83	665.133	76.10	873.976	28.53
Grassland	1.018	1.71	4.399	7.37	11.799	19.76	42.478	71.16	59.695	1.95
Barren land	0.225	0.33	1.750	2.60	12.051	17.91	53.256	79.15	67.282	2.20
Shrubland	0.075	1.53	0.100	2.04	1.234	25.05	3.517	71.39	4.927	0.16
Forest	64.154	3.18	247.586	12.26	758.176	37.54	949.548	47.02	2019.465	65.91
Water body	0.114	0.96	0.549	4.59	1.830	15.31	9.456	79.14	11.949	0.39
Total	76.885	2.53	305.785	10.07	932.155	30.69	1723.389	56.74	3037.292	100.00

**Figure 10.** Potential flash flood risk areas.

The flash flood risk potential areas are spatially presented in the following Figure 10. True colour composite of Sentinel 2 was used to visualize the flood risk areas in Figure 10. We can see northern part of the basin is at high risk of flash flood.

Limitation: This study particularly focuses on the flash flood potential area identification. An important flood type, namely, the inundation flood type, was not included in this paper, which demands further investigations.

5. Conclusions

This study has used morphometric parameters to identify flash flood potential areas in the East Rapti River Basin of Nepal. We used satellite remote sensing data in morphometric analysis for overall flash flood risk evaluation. The geomorphic parameters were used in this study have grouped broadly into four categories: drainage characteristics, basin relief, texture, and geometry. Moreover, rainfall, slope, and drainage density were used to highlight the flash flood pocket areas. Two different risk calculation approaches were used to compare and validate the outcome. Morphometric analysis based on the 30-m SRTM data gives valuable information to identify flash flood hazard potential areas. In terms of population distribution and cropland availability, the sub-basins B, J, L, and K

were the important sub-basins. The result showed that sub-basins B, F, and N are at a very high risk of flash followed by F, I, K, and L basins (high). The identified flood risk sub-basins correspond with the recent past flood records. Unlike inundation and riverbank flooding, flash flood potential is high in the upstream river section, which can be attributed to its steeper slope and excess precipitation. It is concluded that the remote sensing data is of great importance for morphometric analysis at a basin-scale to highlights flash flood potential risk areas. This study also concludes that the growing cities: Hetauda and east Bharatpur, are situated at high-, and very high-risk zones. Considering that the entire basin is not equally prone to flood risk, the city planner should prioritize the potential flood risk areas, with an especial focus on the two major cities of the basin.

Author Contributions: Conceptualization, Til Prasad Pangali Sharma, Jiahua Zhang, and Narendra Raj Khanal; Data curation, Til Prasad Pangali Sharma, Jiahua Zhang, and Foyez Ahmed Prodhana; Formal analysis, Til Prasad Pangali Sharma, Jiahua Zhang, Narendra Raj Khanal, Foyez Ahmed Prodhana, and Lkhagvadorj Nanzad; Funding acquisition, Jiahua Zhang; Methodology, Til Prasad Pangali Sharma, Narendra Raj Khanal, and Pashupati Nepal; Project administration, Da Zhang; Resources, Jiahua Zhang and Pashupati Nepal; Supervision, Jiahua Zhang; Validation, Narendra Raj Khanal; Visualization, Foyez Ahmed Prodhana and Da Zhang; Writing—original draft, Til Prasad Pangali Sharma, Jiahua Zhang, and Pashupati Nepal; Writing—review & editing, Til Prasad Pangali Sharma, Narendra Raj Khanal, Foyez Ahmed Prodhana, Lkhagvadorj Nanzad, and Pashupati Nepal. All authors have read and agreed to the published version of the manuscript.

Funding: This work was jointly supported by the CAS Strategic Priority Research Program (No. XDA19030402), the Natural Science Foundation of China (NO. 41871253, 42071425), and the Taishan Scholar Project of Shandong Province (No. TSXZ201712).

Acknowledgments: The first author would like to acknowledge the Chinese Academy of Sciences (CAS) and the World Academy of Sciences (TWAS) for awarding the CAS-TWAS President Fellowship to accomplish PhD degree. We are thankful to Masoud Jafari SHALAMZARI from Iran, and Madan K. Suwal from Canada for improving the English of this paper. Further, we would like to thank editors and anonymous reviewers for their valuable time and suggestions.

Conflicts of Interest: The authors declare no conflict of interest.

References

1. EM-DAT. The International Disaster Database. Available online: www.emdat.be (accessed on 10 August 2020).
2. Antonetti, M.; Horat, C.; Sideris, I.V.; Zappa, M. Ensemble flood forecasting considering dominant runoff processes—Part 1: Set-up and application to nested basins (Emme, Switzerland). *Nat. Hazards Earth Syst. Sci.* **2019**, *19*, 19–40. [[CrossRef](#)]
3. Saharia, M.; Kirstetter, P.E.; Vergara, H.; Gourley, J.J.; Hong, Y.; Giroud, M. Mapping flash flood severity in the United States. *J. Hydrometeorol.* **2017**, *18*, 397–411. [[CrossRef](#)]
4. Jonkman, S.N. Global perspectives on loss of human life caused by floods. *Nat. Hazards* **2005**, *34*, 151–175. [[CrossRef](#)]
5. Gaume, E.; Bain, V.; Bernardara, P.; Newinger, O.; Barbuc, M.; Bateman, A.; Blaškovičová, L.; Blöschl, G.; Borga, M.; Dumitrescu, A.; et al. A compilation of data on European flash floods. *J. Hydrol.* **2009**, *367*, 70–78. [[CrossRef](#)]
6. Mignot, E.; Li, X.F.; Dewals, B. Experimental modelling of urban flooding: A review. *J. Hydrol.* **2019**, *568*, 334–342. [[CrossRef](#)]
7. Navarro, O.; Restrepo-Ochoa, D.; Munoz-Duque, L.A.; Zapa-Perez, K.; Ameline, A.; Mercier, D.; Fleury-Bahi, G. Determinants of coping strategies in two types of natural hazards: Flash floods and coastal flooding. *Int. J. Disaster Risk Reduct.* **2020**, *46*, 101514. [[CrossRef](#)]
8. Kastridis, A.; Stathis, D. *The Effect of Rainfall Intensity on the Flood Generation of Mountainous Watersheds (Chalkidiki Prefecture, North Greece)*; Springer: Cham, Switzerland, 2017; pp. 341–347.
9. Norbiato, D.; Borga, M.; Esposti, S.D.; Gaume, E.; Anquetin, S. Flash flood warning based on rainfall thresholds and soil moisture conditions: An assessment for gauged and ungauged basins. *J. Hydrol.* **2008**, *362*, 274–290. [[CrossRef](#)]
10. Collier, C.G. Flash flood forecasting: What are the limits of predictability? *Q. J. R. Meteorol. Soc.* **2007**, *133*, 3–23. [[CrossRef](#)]
11. Youssef, A.M.; Pradhan, B.; Hassan, A.M. Flash flood risk estimation along the St. Katherine road, Southern Sinai, Egypt using GIS based morphometry and satellite imagery. *Environ. Earth Sci.* **2011**, *62*, 611–623. [[CrossRef](#)]
12. Costache, R.; Pham, Q.B.; Sharifi, E.; Linh, N.T.T.; Abba, S.I.; Vojtek, M.; Vojteková, J.; Nhi, P.T.T.; Khoi, D.N. Flash-flood susceptibility assessment using multi-criteria decision making and machine learning supported by remote sensing and GIS techniques. *Remote Sens.* **2020**, *12*, 106. [[CrossRef](#)]

13. Diakakis, M.; Andreadakis, E.; Nikolopoulos, E.I.; Spyrou, N.I.; Gogou, M.E.; Deligiannakis, G.; Katsetsiadou, N.K.; Antoniadis, Z.; Melaki, M.; Georgakopoulos, A.; et al. An integrated approach of ground and aerial observations in flash flood disaster investigations. The case of the 2017 Mandra flash flood in Greece. *Int. J. Disaster Risk Reduct.* **2019**, *33*, 290–309. [[CrossRef](#)]
14. Costache, R.; Bui, D.T. Identification of areas prone to flash-flood phenomena using multiple-criteria decision-making, bivariate statistics, machine learning and their ensembles. *Sci. Total Environ.* **2020**, *712*, 136492. [[CrossRef](#)] [[PubMed](#)]
15. WMO. *Manual on Flood Forecasting and Warning*; World Meteorological Organization (WMO): Geneva, Switzerland, 2011.
16. Karki, R.; Hasson, S.U.; Schickhoff, U.; Scholten, T.; Böhner, J. Rising precipitation extremes across Nepal. *Climate* **2017**, *5*, 4. [[CrossRef](#)]
17. Li, L.L.; Yang, J.T.; Wu, J. Future flood risk assessment under the effects of land use and climate change in the tiaoqi basin. *Sensors* **2020**, *20*, 6079. [[CrossRef](#)]
18. Gaume, E.; Borga, M.; Llasat, M.C.; Maouche, S.; Lang, M.; Diakakis, M. *Mediterranean Extreme Floods and Flash Floods*; Institut de Recherche pour le Développement: Marseille, France, 2016; pp. 133–144.
19. Adhikari, K.R. Diagnosis of the East Rapti river basin of Nepal. In *Integrated Water-Resources Management in a River-Basin Context*; International Water Management Institute: Gujarat, India, 2001; p. 57.
20. Terti, G.; Ruin, I.; Gourley, J.J.; Kirstetter, P.; Flamig, Z.; Blanchet, J.; Arthur, A.; Anquetin, S. Toward probabilistic prediction of flash flood human impacts. *Risk Anal.* **2019**, *39*, 140–161. [[CrossRef](#)] [[PubMed](#)]
21. Safarina, A.B.; Karnisah, I.; Permana, A.S. Study of the effect of river basin morphology change on threshold parameters in cimahi flood early warning system. In Proceedings of the 11th Aceh International Workshop and Expo on Sustainable Tsunami Disaster Recovery, Banda Aceh, Indonesia, 10–12 October 2018.
22. Jamsheed, A.; Birkmann, J.; McMillan, J.M.; Rana, I.A.; Feldmeyer, D.; Sauter, H. How do rural-urban linkages change after an extreme flood event? Empirical evidence from rural communities in Pakistan. *Sci. Total Environ.* **2021**, *750*. [[CrossRef](#)] [[PubMed](#)]
23. Zhu, S.N.; Dai, Q.; Zhao, B.R.; Shao, J.Q. Assessment of population exposure to urban flood at the building scale. *Water* **2020**, *12*, 3253. [[CrossRef](#)]
24. Faccini, F.; Luino, F.; Paliaga, G.; Sacchini, A.; Turconi, L.; de Jong, C. Role of rainfall intensity and urban sprawl in the 2014 flash flood in Genoa City, Bisagno catchment (Liguria, Italy). *Appl. Geogr.* **2018**, *98*, 224–241. [[CrossRef](#)]
25. Widiasari, I.; Nugoho, L.E.; Widyawan, W.; Efendi, R. Context-based hydrology time series data for a flood prediction model using LSTM. In Proceedings of the 5th International Conference on Information Technology, Computer, and Electrical Engineering (Icitatee), Semarang, Indonesia, 27–28 September 2018; pp. 385–390.
26. Gaume, E.; Borga, M. Post-flood field investigations in upland catchments after major flash floods: Proposal of a methodology and illustrations. *J. Flood Risk Manag.* **2008**, *1*, 175–189. [[CrossRef](#)]
27. Di Baldassarre, G.; Nardi, F.; Annis, A.; Odongo, V.; Rusca, M.; Grimaldi, S. Brief communication: Comparing hydrological and hydrogeomorphic paradigms for global flood hazard mapping. *Nat. Hazards Earth Syst. Sci.* **2020**, *20*, 1415–1419. [[CrossRef](#)]
28. Manfreda, S.; Leo, M.D.; Sole, A. Detection of flood-prone areas using digital elevation models. *J. Hydrol. Eng.* **2011**, *16*, 781–790. [[CrossRef](#)]
29. Petroselli, A.; Vojtek, M.; Vojtekova, J. Flood mapping in small ungauged basins: A comparison of different approaches for two case studies in Slovakia. *Hydrol. Res.* **2019**, *50*, 379–392. [[CrossRef](#)]
30. Ahmed, A.; Hewa, G.; Alrajhi, A. Flood susceptibility mapping using a geomorphometric approach in South Australian basins. *Nat. Hazards* **2021**, *106*, 629–653. [[CrossRef](#)]
31. Pham, B.T.; Avand, M.; Janizadeh, S.; Phong, T.V.; Al-Ansari, N.; Ho, L.S.; Das, S.; Le, H.V.; Amini, A.; Bozchaloei, S.K. GIS based hybrid computational approaches for flash flood susceptibility assessment. *Water* **2020**, *12*, 683. [[CrossRef](#)]
32. Iosub, M.; Minea, I.; Chelariu, O.E.; Ursu, A. Assessment of flash flood susceptibility potential in Moldavian Plain (Romania). *J. Flood Risk Manag.* **2020**. [[CrossRef](#)]
33. Abdelkareem, M. Targeting flash flood potential areas using remotely sensed data and GIS techniques. *Nat. Hazards* **2017**, *85*, 19–37. [[CrossRef](#)]
34. Rijal, K.P. Comparative study of flood calculation approaches, a case study of East Rapti River Basin, Nepal. *Hydro Nepal J. Water Energy Environ.* **2014**, *15*, 60–64. [[CrossRef](#)]
35. Chalise, S. High mountain hydrology in changing climates: Perspectives from the Hindu Kush-Himalayas. In *Developments in Hydrology of Mountain Areas*; UNESCO: Paris, France, 1997; pp. 23–31.
36. Smakhtin, V.U.; Shilpkar, R.L. *Planning for Environmental Water Allocations: An Example of Hydrology-Based Assessment in the East Rapti River, Nepal*; International Water Management Institute (IWMI): Colombo, Sri Lanka, 2005.
37. Abdel-Fattah, M.; Saber, M.; Kantoush, S.A.; Khalil, M.F.; Sumi, T.; Sefelnasr, A.M. A hydrological and geomorphometric approach to understanding the generation of wadi flash floods. *Water* **2017**, *9*, 553. [[CrossRef](#)]
38. Adan, M.S.G.; Dewan, A.; Zannat, K.E.; Abdullah, A.Y.M. The use of watershed geomorphic data in flash flood susceptibility zoning: A case study of Karnaphuli and Sangu river basin of Bangladesh. *Nat. Hazards* **2019**, *99*, 425–448. [[CrossRef](#)]
39. Hussein, S.; Abdelkareem, M.; Hussein, R.; Askalany, M. Using remote sensing data for predicting potential areas to flash flood hazards and water resources. *Remote Sens. Appl. Soc. Environ.* **2019**, *16*, 100254. [[CrossRef](#)]
40. Vuichard, D.; Zimmermann, M. The Langmoche flash-flood, Khumbu Himal, Nepal. *Mt. Res. Dev.* **1986**, *6*, 90–94. [[CrossRef](#)]
41. Talchabhadel, R.; Sharma, R. Real time data analysis of west Rapti River Basin of Nepal. *J. Geosci. Environ. Prot.* **2014**, *6*, 53–61. [[CrossRef](#)]

42. Sharma, T.P.P.; Zhang, J.H.; Koju, U.A.; Zhang, S.; Bai, Y.; Suwal, M.K. Review of flood disaster studies in Nepal: A remote sensing perspective. *Int. J. Disaster Risk Reduct.* **2019**, *34*, 18–27. [[CrossRef](#)]
43. Dhakal, S. Flood hazard in Nepal and new approach of risk reduction. *Int. J. Landslide Environ.* **2014**, *1*, 13–14.
44. Uddin, K.; Shrestha, H.L.; Murthy, M.S.; Bajracharya, B.; Shrestha, B.; Gilani, H.; Pradhan, S.; Dangol, B. Development of 2010 national land cover database for the Nepal. *J. Environ. Manag.* **2015**, *148*, 82–90. [[CrossRef](#)]
45. Government of Nepal. *National Economic Census 2018 Report*; National Planning Commission, Central Bureau of Statistics: Kathmandu, Nepal, 2020; p. 180.
46. Shukla, A.; Shivakoti, G.; Poudel, R.; Joshi, N. A process documentation study explaining dynamism in water rights in East Chitwan. In Proceedings of the International Conference, Chitwan, Nepal, 17–21 March 1996.
47. WHO. *WHO Methods and Data Sources for Global Burden of Disease Estimates 2000–2011*; World Health Organization (WHO): Geneva, Switzerland, 2013.
48. Noy, I. A global comprehensive measure of the impact of natural hazards and disasters. *Glob. Policy* **2016**, *7*. [[CrossRef](#)]
49. Government of Nepal. *Nepal Disaster Risk Reduction Portal*; Government of Nepal: Kathmandu, Nepal, 2020; Volume 2020.
50. Dewals, B.; Bruwier, M.; Mustafa, A.; Peltier, Y.; Saadi, I.; Archambeau, P.; Erpicum, S.; Orban, P.; Cools, M.; Dassargues, A.; et al. Landuse change and future flood risk: An integrated and multi-scale approach. In Proceedings of the 36th IAHR World Congress, The Hague, The Netherlands, 28 June–3 July 2015; pp. 5105–5116.
51. Shilpakar, R.L.; Bastiaanssen, W.G.; Molden, D.J. A remote sensing-based approach for water accounting in the East Rapti River Basin, Nepal. *Himal. J. Sci.* **2011**, *7*, 15–30. [[CrossRef](#)]
52. Kabenge, M.; Elaru, J.; Wang, H.; Li, F. Characterizing flood hazard risk in data-scarce areas, using a remote sensing and GIS-based flood hazard index. *Nat. Hazards* **2017**, *89*, 1369–1387. [[CrossRef](#)]
53. Strahler, A.N. Quantitative analysis of watershed geomorphology. *Eos Trans. Am. Geophys. Union* **1957**, *38*, 913–920. [[CrossRef](#)]
54. Schumm, S.A. Evolution of drainage systems and slopes in badlands at Perth AMboy, New Jersey. *Geol. Soc. Am. Bull.* **1956**, *67*, 597–646. [[CrossRef](#)]
55. Miller, V.C. *Quantitative Geomorphic Study of Drainage Basin Characteristics in the Clinch Mountain Area, Virginia and Tennessee*; Columbia University: New York, NY, USA, 1953.
56. Horton, R.E. Erosional development of streams and their drainage basins: Hydrophysical approach to quantitative morphology. *Geol. Soc. Am. Bull.* **1945**, *56*, 275–370. [[CrossRef](#)]
57. Strahler, A.N. Part II. Quantitative geomorphology of drainage basins and channel networks. In *Handbook of Applied Hydrology*; McGraw-Hill: New York, NY, USA, 1964; pp. 4–39.
58. Jenks, G.F. The data model concept in statistical mapping. *Int. Yearb. Cartogr.* **1967**, *7*, 186–190.
59. Davis, J.C.; Sampson, R.J. *Statistics and Data Analysis in Geology*; Wiley: Hoboken, NJ, USA, 1986.
60. Gregory, K.J.; Walling, D.E. *Drainage Basin Form and Process: A Geomorphological Approach*; Edward Arnold Publishers Ltd.: London, UK, 1973; p. 456.
61. Faniran, A. The index of drainage intensity—A provisional new drainage factor. *Aust. J. Sci.* **1968**, *31*, 328–330.
62. Yang, L.; Meng, X.; Zhang, X. SRTM DEM and its application advances. *Int. J. Remote Sens.* **2011**, *32*, 3875–3896. [[CrossRef](#)]
63. Ludwig, R.; Mauser, W. Modelling catchment hydrology within a GIS based SVAT-model framework. *Hydrol. Earth Syst. Sci.* **2000**, *4*, 239–249. [[CrossRef](#)]
64. Tarboton, D.G. A new method for the determination of flow directions and upslope areas in grid digital elevation models. *Water Resour. Res.* **1997**, *33*, 309–319. [[CrossRef](#)]
65. Yuan, F.; Zhang, L.M.; Soe, K.M.W.; Ren, L.L.; Zhao, C.X.; Zhu, Y.H.; Jiang, S.H.; Liu, Y. Applications of TRMM- and GPM-era multiple-satellite precipitation products for flood simulations at sub-daily scales in a sparsely gauged watershed in Myanmar. *Remote Sens.* **2019**, *11*, 140. [[CrossRef](#)]
66. Zhao, T.B.; Yatagai, A. Evaluation of TRMM 3B42 product using a new gauge-based analysis of daily precipitation over China. *Int. J. Climatol.* **2014**, *34*, 2749–2762. [[CrossRef](#)]
67. Shi, Y.F.; Li, L.; Zhang, L.L. Application and comparing of IDW and Kriging interpolation in spatial rainfall information. In Proceedings of the Geoinformatics 2007: Geospatial Information Science, Nanjing, China, 25–27 May 2007. [[CrossRef](#)]
68. Capolongo, D.; Refice, A.; Bocchiola, D.; D’Addabbo, A.; Vouvalidis, K.; Soncini, A.; Zingaro, M.; Bovenga, F.; Stamatopoulos, L. Coupling multitemporal remote sensing with geomorphology and hydrological modeling for post flood recovery in the Strymonas dammed river basin (Greece). *Sci. Total Environ.* **2019**, *651*, 1958–1968. [[CrossRef](#)]
69. Haggett, P.; Chorley, R.J. *Network Analysis in Geography*; Edward Arnold Publishers Ltd.: London, UK, 1969.
70. Chorley, R.J.; Malm, D.E.G.; Pogorzelski, H.A. A new standard for estimating drainage basin shape. *Am. J. Sci.* **1957**, *255*, 138–141. [[CrossRef](#)]
71. Marafuz, I.; Rodrigues, C.; Gomes, A. Analysis and assessment of urban flash floods on areas with limited available altimetry data (Arouca, NW Portugal): A methodological approach. *Environ. Earth Sci.* **2015**, *73*, 2937–2949. [[CrossRef](#)]
72. Kastridis, A.; Stathis, D. Natural and anthropogenic flash flood generation in mountainous watersheds—The case of Apollonia torrent. In Proceedings of the Protection and Restoration of the Environment XI. Water Resources Management, Thessaloniki, Greece, 3–6 July 2012; pp. 126–135.